High frequency electro optic measurement of strained silicon racetrack resonators

Massimo Borghi[1a], Mattia Mancinelli [a], Florian Merget [b], Jeremy Witzens[b], Martino Bernard [c], Mher Ghulinyan [c], Georg Pucker [c] and Lorenzo Pavesi [a]

[a]Department of Physics, Nanoscience Laboratory, University of Trento, I-38123 Povo, Italy
[b]Institute of Integrated Photonics, RWTH Aachen University, Sommerfeldstr. 24, D-52074, Aachen
[c]Centre for Materials and Microsystems, Fondazione Bruno Kessler, I-38123 Povo, Italy

ABSTRACT

In this paper, we report on time resolved electro-optic measurements in strained silicon resonators. Strain is induced by applying a mechanical deformation to the device. It is demonstrated that the linear electro-optic effect vanishes when the applied voltage modulation varies much faster than the free carrier lifetime, and that this occurs independently on the level of the applied stress. This demonstrates that, at frequencies which lie below the free carrier recombination rate, the electro-optic modulation is caused by plasma carrier dispersion. After normalizing out free carrier effects, it is found an upper limit of (8 ± 3) pm/V to the value of the strain induced $\chi^{(2)}_{eff,zzz}$ tensor component. This is an order of magnitude lower than the previously reported values for static electro-optic measurements.

Keywords: Strained silicon, Pockels effect, Plasma carrier effect, Integrated optical devices, Electro-optic modulators.

1. INTRODUCTION

The linear electro-optic effect (or Pockels effect), that is the change of the refractive index in response to an applied electric field, is absent in silicon. This is due to the Si symmetry. The enabling of an appreciable $\chi^{(2)}$ in Si would validate the Silicon-On-Insulator (SOI) platform as an alternative to Lithium Niobate for second-order nonlinear optics. In the last few years, strained Silicon has been proposed as a potential electro-optic material [1]. The centrosymmetry of the crystal is broken by a stressing film, usually Silicon Nitride (Si_xN_x), which is deposited on the top of the waveguides. Typically, the presence of a strain induced $\chi^{(2)}$ has been investigated in integrated unbalanced Mach-Zehnder interferometers, in which one or both arms are driven by a low frequency (KHz regime) AC electric field. As a consequence of the electro-optic effect, the fringes at the output of the interferometer shifts. From the amount of this shift, and from the knowledge of the device geometry, the $\chi^{(2)}$ tensor components can be extracted. By following this approach, several demonstrations of electro-optic modulation have been reported [2,3]. Typically, the value of the strain induced $\chi^{(2)}$ ranged from 15 pm/V [1] to 336 pm/V [3]. In all these works, the linear relation between the applied field and the effective index change has been considered as the proof of the presence of the Pockels effect. However, as recently reported [4], a linear effective index variation of the optical mode in the waveguide can be also induced by the injection of free carriers localized at the interface between Si and Si_xN_x. As a consequence, the magnitude of the extracted $\chi^{(2)}$ components can be overestimated by the contribution of plasma carrier dispersion to the electro-optic modulation. A method which allows to distinguish free carrier effects from the ones arising by second order nonlinearities is based on time resolved electro-optic measurements. The modulation speed of free carriers is limited by their lifetime in the waveguide, which is of the order of few nanoseconds. On the contrary, the effective index change

[1]massimo.borghi@unitn.it

Silicon Photonics and Photonic Integrated Circuits V, edited by Laurent Vivien, Lorenzo Pavesi, Stefano Pelli,
Proc. of SPIE Vol. 9891, 98910D · © 2016 SPIE · CCC code: 0277-786X/16/$18 · doi: 10.1117/12.2227561

induced by $\chi^{(2)}$ nonlinearities follows instantaneously the applied electric field up to optical frequencies. In this work, we performed high frequency measurements of the electro-optic effect in strained silicon racetrack resonators. Strain is applied by a mechanical deformation of the sample. We performed a sweep of the modulation frequency from 50 MHz up to 5 GHz, which lies above the measured free carrier recombination rate. We demonstrated that the amplitude of the electro-optic modulation monotonically decreases with frequency, and that the magnitude of the $\chi^{(2)}_{eff,zzz}$ tensor component do not change appreciably with strain, which allowed us to conclude that free carriers are the responsible of the observed behavior. An upper limit of $\chi^{(2)}_{eff,zzz}$ = (8 ± 3) pm/V has been set to the high frequency value of the $\chi^{(2)}$, which corresponds to the noise level of our measuring apparatus. This value is an order of magnitude lower than the previously reported values for static electro-optic measurements.

2. DEVICE DESIGN AND EXPERIMENTAL SETUP

The electro-optic effect is investigated in the device shown in Fig.1(a). It is a racetrack resonator in the Add-Drop filter configuration, which is patterned on a 6'' Silicon-On-Insulator wafer using 293 nm UltraViolet lithography.

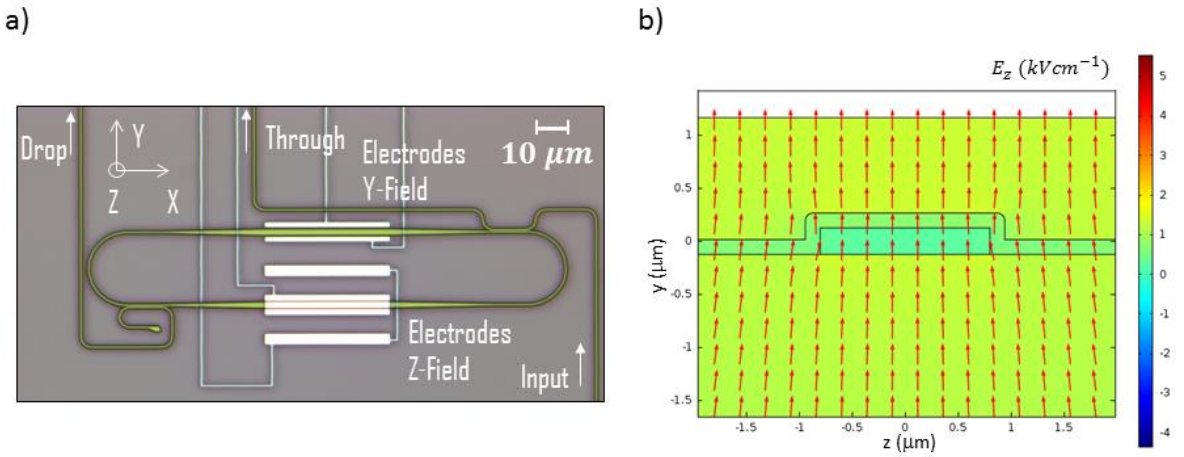

Figure 1. (a) Optical microscope image of the racetrack resonator. The device is excited by sending light to the Input port, while the transmitted and reflected signals are recorded in the Through and Drop ports respectively. Two set of electrodes are present, one allows to apply an electric field in the y-direction (Electrodes Y-field), while the other one in the z-direction (Electrodes Z-field). In this experiment, only the Z-field set is used. (b) FEM simulation of the electric field distribution inside the waveguide core when 1 V is applied to the electrodes.

The thickness of the silicon layer is 250 nm. A layer of Si_3N_4 of 140 nm thickness has been conformally deposited on the top of the waveguides by Low Pressure Chemical Vapor Deposition to reproduce the experimental conditions described in Refs. [2,3,4]. The residual stress on the Si_3N_4 layer, after the silica deposition, has been measured to be -0.19 GPa. The height of the lower and upper silica cladding are 3 μm and 900 nm respectively. The perimeter of the resonator is 415 μm and the coupling coefficient with the bus waveguides is κ^2 = 0.07. The resonator waveguide has a width of 400 nm, which is adiabatically tapered to a width of 1.6 μm in the regions where the electric field is applied. This is achieved by using a set of three electrodes, as shown in Fig.1(a) (Z-field set): the central one is grounded, while the two adjacent electrodes are shorted to a common voltage. The magnitude of the electric field in the waveguide core has been computed through Finite Element Method (FEM) simulations. When 1 V is applied between the electrodes, the electric field has an average value of 0.25 kV/cm inside the waveguide core. Fig.1(b) shows the result of this simulation. The experimental setup is shown in Fig.2(a). Light from a C-band Infra-Red laser amplified by an EDFA is edge coupled to the input port of the resonator using a polarization maintaining lensed fiber (PMF). The light polarization is set to TM. A nanometric XYZ positioning stage is used to minimize the coupling losses. The transmitted light from the resonator Through port is split: 10 % is sent to a reference photodiode, while 90% feeds a high-bandwidth photoreceiver (43 GHz) connected to a vector network analyzer (VNA). The VNA also provides a 28 dBm (after amplification) sinusoidal

voltage modulation to the electrodes, using impedance matched Tungsten tips with 40 GHz bandwidth. The sample is strained by a mechanical deformation through a special sample holder. This is shown in Fig.2(b). The device is fixed on a sample holder that can provide a variable stress, adjusted by rotating a 250 μm pitch. The pressure exercised by the screw bends the sample (see Fig.3(a)).

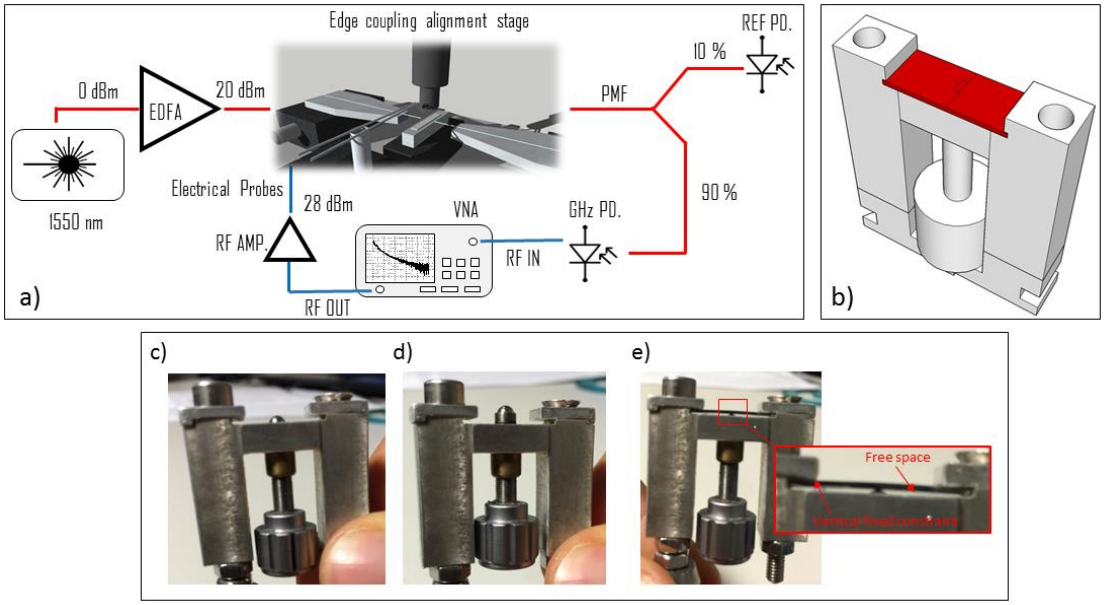

Figure 2. (a) Experimental setup used for the electro-optic measurements. PMF = polarization maintaining fibers; PD = photodiodes; VNA = vector network analyzer, RF IN(OUT) = Radio frequency IN(OUT). (b) 3D model of the stressing sample holder. The sample is indicated in red. (c-d) Stressing sample holder with the screw set at two different displacements. (e) Stressing sample holder with the Silicon chip mounted on it. The inset shows that the sample is not touching the Alluminium surface. The contact lines between the holder and the sample, which constitute a fixed constraint on the vertical direction, are also indicated.

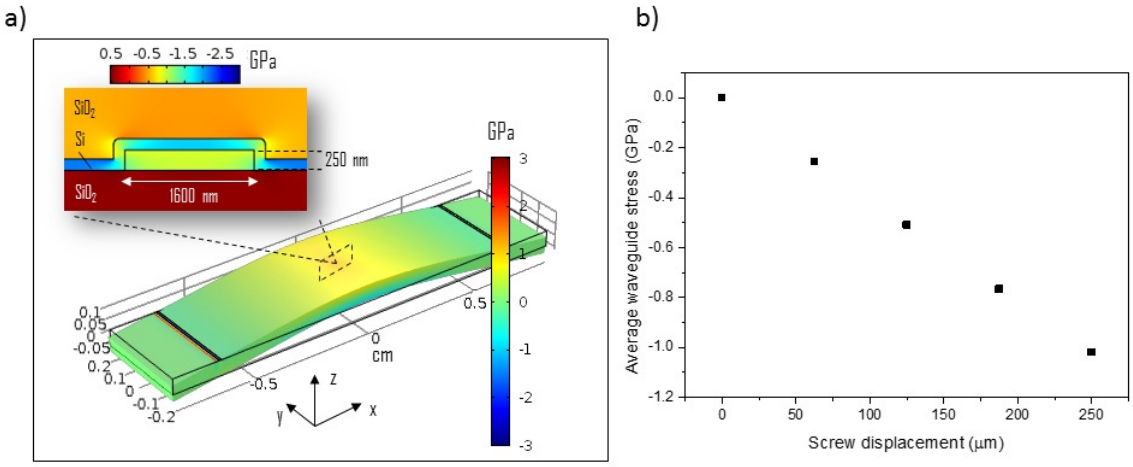

Figure 3. (a) Finite element simulation of the stress distribution (σ_{xx} element of the stress tensor σ_{ij}) on the sample subjected to a 62.5 μm screw displacement. The discontinuities near the ends are due to the line contact with the sample holder (see Fig.2(e)), which lies 2 mm from the end. The inset shows the stress profile along the waveguide cross section. (b) Average stress (σ_{xx}) inside the waveguide as a function of the screw displacement.

It is possible to displace the screw by approximately its complete pitch before breaking the chip. To avoid micro fractures, the screw displacements are kept lower than 150 μm. The reason why the mechanical sample holder is used is to examine the behavior of the electro-optic modulation as a function of different stress levels at high frequencies, where free carrier effects should be not present. In this way it is possible to investigate the dependence of the $\chi^{(2)}$ tensor components as a function of the applied strain. The strain is mechanically induced since the sample ends are fixed to the holder, while the screw pushes the center of the sample. The relationship between the screw displacement and the stress induced inside the waveguide is computed from FEM computations. The results are shown in Fig.3(a,b). Only the σ_{xx} element of the stress tensor σ_{ij} is plotted, since it was found to be one order of magnitude higher than the σ_{yy} component and five orders of magnitude higher than the remaining tensor elements. In the region where the resonator is located (dashed rectangle in Fig.3(a)), the overall stress distribution can be approximated as compressive and uniaxial in the x-direction. In Fig.3(b), it is shown the linear relationship between the screw displacement and the computed average stress in the waveguide. The stress magnitude and direction are comparable to the ones used in other experiments [2,3,4]. As it can be appreciated in Fig.3(a) (inset), it exists a large stress (hence strain) gradient at the interface between Si and Si_3N_4, where the overlap with the TM optical mode is maximum. This feature is essential since a homogeneous strain does not break the centrosymmetry of the crystal.

3. EXPERIMENTAL RESULTS

At first, the screw displacement is set to zero, so no stress (except the residual one due to the Si_3N_4 layer) is applied to the waveguide. By monitoring the output signal at the reference photodiode, the laser wavelength is tuned near the -3 dB point of one of the resonances (Fig.4, inset), where the sensitivity to small refractive index variations is maximized. The quality factor of this resonance is Q = 23200. The sinusoidal modulation is then applied to the sample electrodes using the VNA and a 32 dB electrical amplifier (see Fig.2(a)). With reference to Fig.1(a), both the optical field and the static electric field lie in the z-direction. As a result of the bias modulation, the resonance oscillates back and forth with respect to the laser wavelength, inducing a periodic modulation of the transmitted optical signal I_{out} at the Through port of the resonator. When the input laser wavelength λ is tuned near one of the resonance wavelengths λ_0 of the resonator, the Through intensity I_{out} can be approximated by the following expression:

$$I_{out} \approx K\left(1-\frac{A\gamma^2}{\gamma^2+\left(\lambda-\lambda_0\right)^2}\right) \tag{1}$$

in which A is proportional to the extinction rate of the resonance, K is a constant which depends on the experimental setup and 2γ is the full width at half maximum of the Lorentzian. The resonance wavelength is a function of the modulation voltage $V(t)=V_0\sin(\omega t)$, since this changes the effective index through the electro-optic effect. As a consequence, the Through intensity varies in time, following the differential equation:

$$\frac{dI_{out}}{dt}=\frac{\partial I_{out}}{\partial\lambda_0}\frac{d\lambda_0}{dV}\frac{dV}{dt} \tag{2}$$

The relation between the voltage $V(t)$ and the resonance wavelength λ_0 is given by:

$$\lambda_0=\bar{\lambda}_0\left(1+\frac{\Delta n_{eff}(V(t))L_e}{n_g L_{tot}}\right) \tag{3}$$

in which $\bar{\lambda}_0$ is the resonance wavelength when no voltage is applied, Δn_{eff} is the effective index change induced by the electro-optic effect, L_e is the length of the region where the voltage is applied, L_{tot} is the resonator length and n_g is the modal group index.

The effective index change associated to the linear electro-optic effect, when a field $E_{DC} = \alpha V$ is applied, is given by [5]:

$$\Delta n_{eff} = \frac{\chi^{(2)}{}_{eff,zzz} n_g E_{DC}}{2 n_c{}^2} \tag{4}$$

in which n_c is the refractive index of the core material of the waveguide. The modal averaged tensor component $\chi^{(2)}{}_{eff,zzz}$ is defined as:

$$\chi^{(2)}{}_{eff,zzz} = \frac{\int_{core} \chi_{zzz}{}^2(x,y) n^2(x,y) |e_z(x,y)|^2 \, dxdy}{\int n^2(x,y) |e(x,y)|^2 \, dxdy} \tag{5}$$

in which n is the refractive index profile of the waveguide, $\chi_{zzz}{}^{(2)}$ is the second order nonlinearity in the material and $e(x,y)$ is the modal optical field profile. In writing the expression in Eq.(5), the optical field has been assumed to be mainly polarized along the z-direction, so that all the other components of the $\chi^{(2)}$ tensor do not contribute to the integral at the numerator. By combining together Eq.(1) through Eq.(4), the oscillation amplitude I_{out} can be written as:

$$I_{out} = K \frac{\partial I_{out}}{\partial \lambda_0} \frac{\bar{\lambda}_0 L_e \chi^{(2)}_{eff,zzz} E_{DC}}{2 L_{tot} n_c^2} \tag{6}$$

The quantity I_{out} is what is actually recorded by the VNA. The magnitude of the $\chi^{(2)}{}_{eff,zzz}$ component can be extracted from Eq.(6), since all the other parameters can be directly measured from the experiment or computed through FEM simulations. Three different stress levels, corresponding to 0 GPa (no stress), -0.24 GPa and -0.48 GPa, are applied, and for each of them the $\chi^{(2)}{}_{eff,zzz}$ component is measured as a function of the modulation frequency. This is swept from 50 MHz to 5 GHz. The result of this measurement is shown in Fig.4.

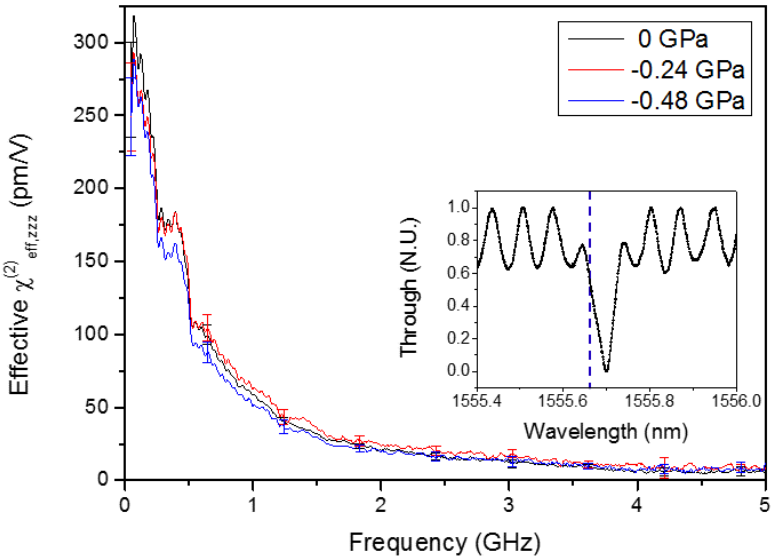

Figure 4. Effective $\chi^{(2)}{}_{eff,zzz}$ as a function of the electrical modulation frequency for three different stress levels in the waveguide. For clarity, the errors are reported only for certain points of the curves. The inset shows the working point of the electro optic measurement. The black line denotes the Through transmission, while the vertical blue dashed line represents the wavelength of the laser.

As can be seen, the value of $\chi^{(2)}_{eff,zzz}$ is maximum in the low frequency range and it decreases as the modulation frequency increases. The extracted value of the $\chi^{(2)}_{eff,zzz}$ close to the DC regime is ~270 pm/V, which is comparable to values reported in the literature for static electro-optic measurements using the same electric field and optical polarization directions [2,3]. The frequency cut-off of the modulation, i.e., the frequency at which the $\chi^{(2)}_{eff,zzz}$ halves, is ν_c = (0.50 ± 0.01) GHz, corresponding to a time constant of τ_c = (0.55 ± 0.01) ns. The minimum value of the $\chi^{(2)}_{eff,zzz}$ that can be detected is limited by the electrical noise floors of the VNA and of the photoreceiver. This corresponds to an effective $\chi^{(2)}_{eff,zzz}$ of (8 ± 3) pm/V. Very slight differences are observed by changing the stress level. These results clearly show that the modulation cannot be attributed to a strain-induced $\chi^{(2)}$. In fact, if the latter was the cause for the observed effect, one would expect the transmitted signal to follow the voltage variations instantaneously up to optical frequencies. Rather, the signal modulation is related to a slower dispersion mechanism, with a characteristic time in the nanosecond scale. This confirms the results reported in Ref. [4], in which the electro-optic modulation has been attributed to free carrier dispersion. To exclude the possibility that the bandwidth of the electro-optic modulation is limited by the photon lifetime in the cavity, we tuned the laser wavelength on resonance, and we modulated the input signal in time using a Lithium Niobate electro-optic modulator. We then recorded the Drop intensity as the frequency of the modulation is swept from 500 MHz to 5 GHz. This is shown in Fig.5(a).

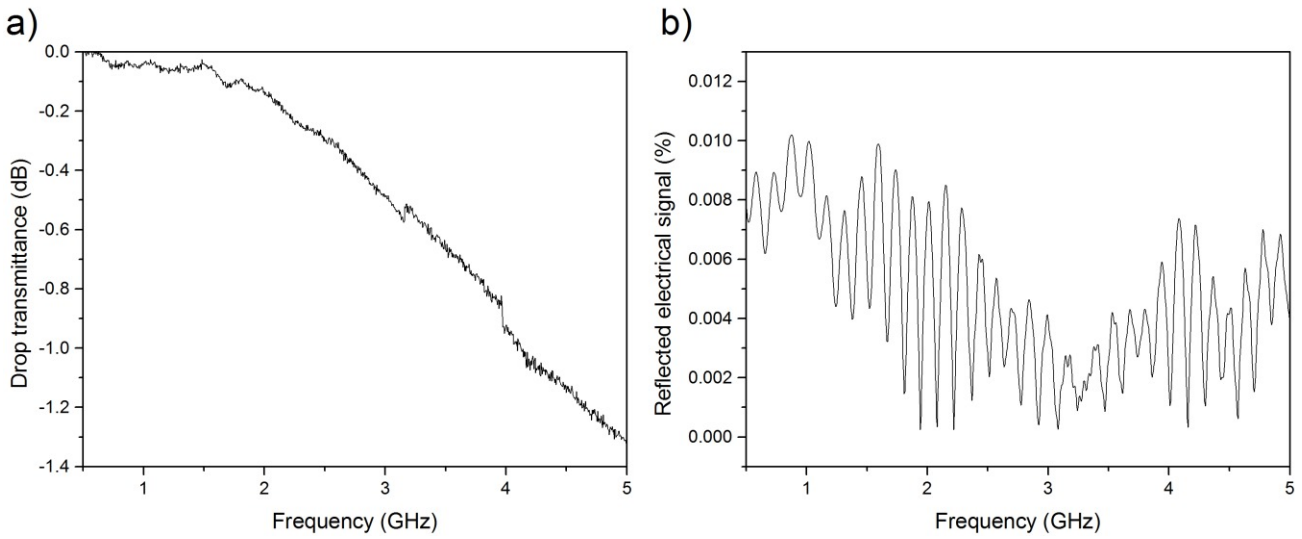

Figure 5. a) Amplitude of the Drop intensity variations as a function of the frequency of the input optical signal. (b) Percentage of the electrical power which is reflected back towards the VNA from the Tungsten tips as a function of the voltage modulation frequency.

The signal decreases of about -1.3 dB from 500 MHz to 5 GHz, indicating that the cavity is far from its optical cut-off in the investigated frequency range. This means that the decrease of the effective $\chi^{(2)}$ with frequency can not be attributed to the photon lifetime in the cavity. We also checked that the voltage at the output of the VNA is transferred without significant attenuation or reflections to the Tungsten tips. This is done by measuring the percentage of electrical power which is reflected back to the VNA. The result is shown in Fig.5(b), and it indicates that less than the 0.01% of the input electrical power is reflected. As a last step, we measured the free carrier lifetime τ inside the waveguide, in order to check its consistency with the characteristic timescale τ_c of the electro-optic modulation found in the high frequency measurement shown in Fig.4. This is done by using a pump and probe scheme, in which an intense laser pulse of 40 ps duration (100 MHz repetition rate) is coupled to the waveguide, and the time-dependent losses of a weaker continuous wave (CW) probe beam are monitored. The experimental setup is shown in Fig.6(a). The wavelength of the pulsed laser is fixed to 1.55 μm, while the one of the CW probe can be tuned, and it is set to 1.560 μm. A bandpass filter, placed at the output of the sample, allows to filter out the pump and monitor only the CW laser. The short pump pulse generates

free carriers due to TPA; these free carriers in turn attenuate the probe signal due to free-carrier absorption. After switching off the pump laser, the probe beam transmission slowly recovers due to free carrier recombination or diffusion away from the spot of the pump laser. The effective free carrier lifetime can then be extracted from the time-resolved measurement of the recovering probe beam transmission. The result is shown in Fig.6(b). The sudden signal decrease is due to the pulse arrival and, consequently, to TPA carrier generation. The subsequent slower signal recovery is due to the finite free carrier lifetime. From these data, a carrier life time of τ = (1.06 ± 0.01) ns has been estimated. Being $\tau \approx \tau_c$, this constitutes another proof that the observed modulation can be attributed to plasma carrier dispersion.

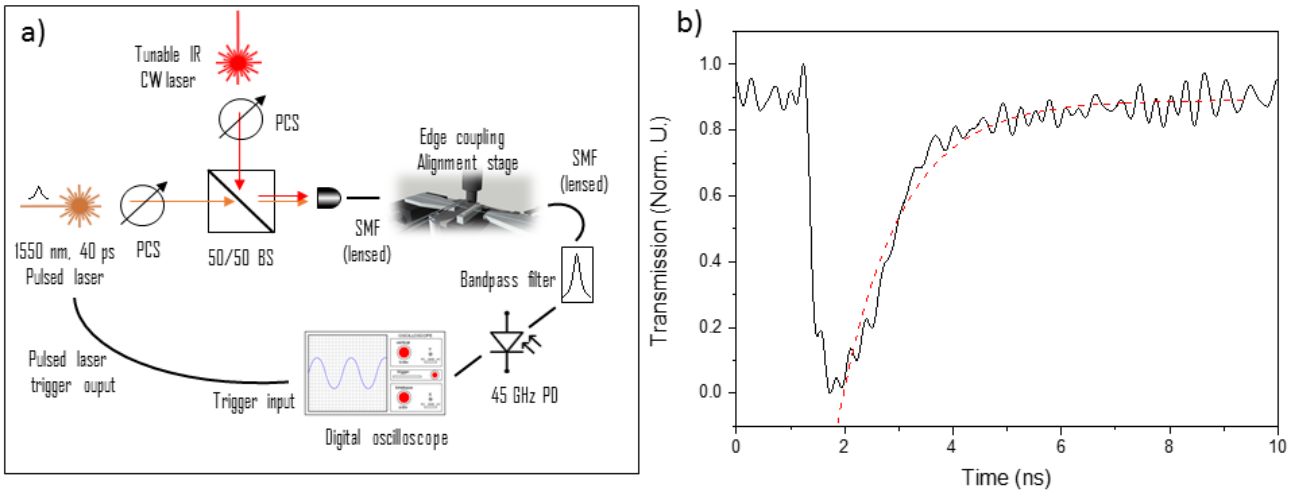

Figure 6. a) Sketch of the experimental setup used to measure the free carrier lifetime in the waveguide. PCS = Polarization Controlling Stage, BS = Beamsplitter, SMF = Single Mode Fiber, PD = Photodetector. (b) Measurement of the carrier lifetime. The black line is the Drop signal (in normalized units) in time, while the red dotted line is an exponential fit of the rising edge.

4. CONCLUSIONS

In this work, we performed high frequency electro-optic measurements of strained silicon racetrack resonators, with the aim to isolate the contribution due to free carriers to the one arising from second order nonlinearities to the linear electro-optic effect. This is done on the basis of the different timescales at which the two dispersion mechanisms act. We found that the amplitude of the electro-optic modulation decreased as the frequency of the applied electric field is increased, with a cut-off frequency in the GHz regime. This behaviour is found to be independent on the level of applied stress. These results rule out any contribution arising from the second order nonlinearity to the electro-optic modulation, indicating that, at the low frequency (KHz-MHz regime), plasma carrier dispersion is the responsible for the observed modulation. We extracted an upper limit of (8 ± 3) pm/V for the strain-induced $\chi^{(2)}$ in Si waveguides at -0.48 GPa of applied stress, which corresponds to our minimum detectable signal. This value is more than one order of magnitude lower than the one reported in the low-frequency regime in the literature.

REFERENCES

[1] Jacobsen, Rune S., et al., "Strained silicon as a new electro-optic material.", Nature, 441, 199-202, (2006).
[2] Chmielak, B., et al., "Pockels effect based fully integrated, strained silicon electro-optic modulator.", Opt. Express, 19, 17212-17219, (2011).
[3] Damas, P., et al., "Wavelength dependence of Pockels effect in strained silicon waveguides.", Opt. Express, 22, 22095-22100, (2014).

[4] Azadeh, S. S., Merget, F., Nezhad, M. P., and Witzens, J., "On the measurement of the Pockels effect in strained silicon.", Opt. Lett., 40, 1877-1880, (2015).
[5] Borghi, M., et al., "High-frequency electro-optic measurement of strained silicon racetrack resonators", Opt. Lett., 40, 5287-5290, (2015).